

# Chaotic Classical Scattering and dynamics in oscillating 1D potential wells.

G.A. Luna-Acosta<sup>1</sup>, G. Orellana-Rivadeneira,<sup>1</sup> A. Mendoza-Galván,<sup>2</sup> and C. Jung<sup>3</sup>

<sup>1</sup> *Instituto de Física, Universidad Autónoma de Puebla, Apdo. Postal J-48 Pue. 72570, México*

<sup>2</sup> *Centro de Investigacion y de Estudios Avanzados del IPN, Unidad Queretaro, Apdo. Postal 1-798, 76001 Querétaro, México.*

<sup>3</sup> *Centro de Ciencias Físicas, Universidad Nacional Autónoma de Mexico, Apdo. Postal 139-B, 62191, Cuernavaca, Mexico*

October 24, 2018

## Abstract

We study the motion of a classical particle interacting with one, two, and finally an infinite chain of 1D square wells with oscillating depth. For a single well we find complicated scattering behavior even though there is no topological chaos due to the absence of hyperbolic periodic orbits. In contrast, for two coupled square wells there is chaotic scattering. The infinite oscillating chain yields the generic transition to chaos, with diffusion in energy and in space, as the separation between wells is increased. We briefly discuss the relevance of our results to solid state physics.

PACS: 05.45.+b, 03.20

## 1 Introduction

Most of our knowledge about molecular, atomic, and elementary particle physics comes from the analysis of scattering experiments. The potential fields producing the scattering may be the result of one or many particles and may be autonomous or time-dependent. Time-dependent scattering is particularly important nowadays in investigations of transport properties in microscopic and mesoscopic physics, where systems are usually modeled by simple Hamiltonians (see, e.g., [1]- [5]). In this type of systems the description is generally performed using the Schrödinger equation since the devices under consideration are assumed to operate predominantly in the pure quantum limit. However, in order to get the complete picture of motion, it is necessary to study also their classical motion, and the analysis of the quantum-classical correspondence is especially interesting when the classical motion becomes chaotic under certain conditions [6].

The study of the manifestations of chaos in the trans-

port properties of mesoscopic systems has yielded important results. For example, measurements of magnetoresistance in ballistic microstructures in the shape of a chaotic billiard and circle showed clear distinctions in the power spectrum of universal conductance fluctuations and in the line shape of the weak localization peak ([7],[8]). In [9] a criterion was proposed to distinguish between regular and chaotic dynamics by measuring classical resistivity in a type of mesoscopic channels. These results concern time independent phenomena. Here we report preliminary results in the study of the classical dynamics of a type of simple time-dependent systems whose quantum counterparts are models of microscopic or mesoscopic systems. Specifically, we consider the scattering of classical particles interacting with one and two 1D square wells with periodically oscillating depth. The square wells may represent the conduction band defined by a  $Al_xGa_{1-x}As - GaAs$  heterostructure or a quantum dot (see, e.g., [10], [11]) and the oscillating depth may represent the electron-phonon interaction [12] or the presence of a monochromatic elec-

tromagnetic or acoustic field ([4],[10],[13]). We will also consider the dynamics of a classical particle interacting with a chain of oscillating wells. Since the chain is infinite and periodic the system is no longer an open system; the dynamics is recurrent in phase space. This system is the classical counterpart of a particle in a vibrating Kronig-Penney potential. The static Kronig-Penney potential in its quantum version has been fundamental in the understanding of solid state properties (see, e.g., [14]), while its classical version is trivial. However, as will be shown below, when the chain vibrates the classical motion becomes chaotic.

The organization of the paper is as follows. In sections II and III, respectively, we study the scattering of particles off one and two oscillating wells. In Section IV, we consider the oscillating chain and in Section V we draw conclusions.

## 2 A single oscillating well

We consider classical particles interacting with the localized time-dependent potential,

$$V(x, t) = \begin{cases} V_0 & x < 0, x > a \\ D \cos(\omega t) & 0 \leq x \leq a, \end{cases} \quad (1)$$

where  $a$  is the width of the well of height  $V_0$ ,  $\omega$  is the frequency of oscillation of the bottom of the well, and  $D$  is its amplitude (See Fig. 1). We shall only consider the case  $D \leq V_0$ . Assume a particle approaches the well from the left, as indicated in Fig. 1, with kinetic energy  $K_0$ . At time  $t = t_0$  the particle crosses the boundary  $x = 0$  and the bottom of the well has a height  $D \cos(\omega t_0)$ . At that instant its kinetic energy changes abruptly to  $K^* = E_0 - D \cos(\omega t_0)$ , where  $E_0 = K_0 + V_0$ . Since there is no gradient of  $x$  within the well, the ‘‘internal’’ kinetic energy  $K^*$  is conserved while moving inside the well. After a time  $t = t^* = a/p^*$ , with  $p^* = \sqrt{2K^*}$  the particle reaches the right hand side of the well ( $x = a$ ), its total energy being  $E_1 = K^* + D \cos[\omega(t_0 + t^*)]$ . If  $E_1 \geq V_0$  the particle exits to the right with energy

$$E_1 = E_0 + D(\cos\phi_1 - \cos\phi_0), \quad (2)$$

where

$$\phi_1 = \phi_0 + \Delta\phi_0, \quad \phi_0 = \omega t_0 \quad \text{and} \quad (3)$$

$$\Delta\phi_0 \equiv \omega t^* = \omega a / \sqrt{2(E_0 - D \cos\phi_0)} \quad (4)$$

It is convenient to obtain dimensionless energies by rescaling with respect to the height of the well  $V_0$ :

$$\epsilon_1 = \epsilon_0 + \eta_1(\cos\phi_1 - \cos\phi_0) \quad (5)$$

$$\phi_1 = \phi_0 + \eta_2 / \sqrt{\epsilon_0 - \eta_1 \cos\phi_0}, \quad (6)$$

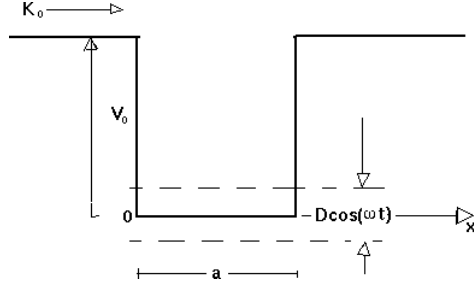


Figure 1: Schematic of the 1D oscillating well.  $V_0$  is the static depth and  $K_0$  is the kinetic energy of the incoming particle.

where  $\epsilon \equiv E/V_0$ ,

$$\eta_1 \equiv D/V_0, \quad (7)$$

and

$$\begin{aligned} \eta_2 &\equiv 2\pi\omega/\omega_c, \\ \omega_c &\equiv 2\pi/T_c, \quad \text{and} \\ T_c &\equiv a/\sqrt{2V_0}. \end{aligned} \quad (8)$$

Note that  $T_c$  is the time for a particle with total energy  $V_0$  to cross the well in the absence of oscillations.

Equation (5) makes sense as long as  $\epsilon_1 \geq 1$ . If  $\epsilon_1 < 1$ , the particle reflects at  $x = a$  without changing its internal kinetic energy  $K^*$ . The particle then will reach  $x = 0$  with energy and phase given by

$$\begin{aligned} \epsilon_2 &= \epsilon_0 + \eta_1(\cos\phi_2 - \cos\phi_0) \\ \phi_2 &= \phi_1 + \Delta\phi_0 = \phi_0 + 2\Delta\phi_0, \end{aligned} \quad (9)$$

where

$$\Delta\phi_0 = \eta_2 / \sqrt{\epsilon_0 - \eta_1 \cos\phi_0} \quad (10)$$

Again, if  $\epsilon_2 < 1$  the particle will reflect towards  $x = a$  and so on, until for some number  $N$  of collisions with the boundaries, the energy  $\epsilon_N$  becomes greater or equal to 1. The critical value  $\epsilon_N = 1$  implies that the particle exits the well but with zero kinetic energy. Thus, the scattering map is given by

$$\begin{aligned} \epsilon_N &= \epsilon_0 + \eta_1(\cos\phi_N - \cos\phi_0) \geq 1 \\ \phi_N &= \phi_0 + N\eta_2 / \sqrt{\epsilon_0 - \eta_1 \cos\phi_0} \end{aligned} \quad (11)$$

This map is deceptively simple. Clearly, if  $\epsilon_0 \geq 1 + 2\eta_1$  then  $\epsilon_1 \geq 1$  and the particle will certainly be transmitted with phase and energy given by Eq.(11) with  $N = 1$ . However, if  $\epsilon_0 < 1 + 2\eta_1$ , then  $\epsilon_1$  can be less than one, depending on the initial phase, and one cannot simply substitute  $\phi_N$  into  $\epsilon_N$  to determine the fate of the scattered particle, i.e., whether it was transmitted or reflected and with what energy. It is necessary to calculate  $\phi_n$  and  $\epsilon_n$  sequentially for  $n = 1, 2, 3 \dots N$  to discover after how many collisions  $N$  the condition  $\epsilon_N \geq 1$  is satisfied.

In order to get a panorama of the type of scattering asymptotes that can be obtained for typical values of  $\eta_1$  and  $\eta_2$ , it is useful to construct a hierarchy level plot where each level corresponds to a given number of collisions and the domain is the set of all incoming asymptotes [15]. Such a hierarchy plot is shown in Fig. 2, for the parameters  $\eta_1 = 0.5$  and  $\eta_2 = 16.45$ . This plot is typical of small to moderate frequencies of oscillations ( here  $\eta_2 = 16.45$ , i.e.,  $\omega \approx 2.6\omega_c$ ). (For higher frequencies of oscillation of the well, the hierarchy plots show increasingly complicated structures). The boundaries between the level 1 and any other level  $N$  are given by the set of initial conditions  $(\epsilon_0, \phi_0)$  that yield outgoing energies  $\epsilon_N = 1$ . One may be tempted to obtain this set of  $(\epsilon_0, \phi_0)$  by inverting map (11) and using  $\epsilon_N = 1$ , but knowledge of the final phase  $\phi_N$  is lacking. However, the following procedure enables us to obtain this set. First we apply map (11) to the conditions  $\epsilon_0 = 1$  and any  $\phi_0$  in  $-\pi \leq \phi_0 \leq \pi$ . This produces the outgoing values  $(\epsilon_n, \phi_n)$  for some integer  $n$ . Then it is easy to show, considering the symmetry of the cosine function, that forward iteration of  $(\epsilon_n, -\phi_n)$  yields the desired result  $\epsilon = 1$ . Hence, the initial conditions on the boundaries, or separatrices, between hierarchy levels are given by the set  $(\epsilon_n, -\phi_n)$  thus defined. Figure 3 shows the result of this procedure for a set of 6,000 values of initial phases in the range  $-\pi \leq \phi_0 \leq \pi$ .

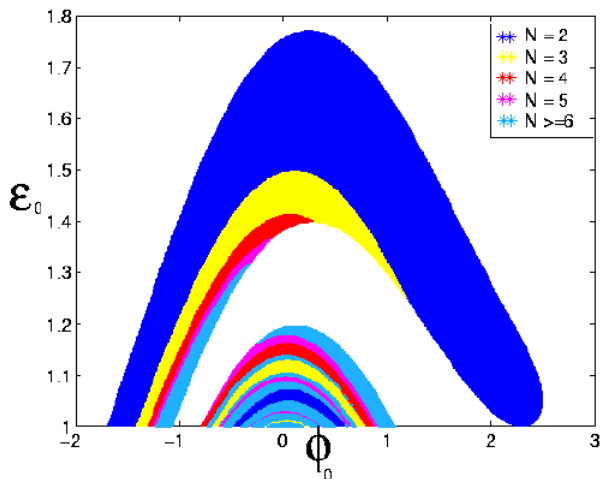


Figure 2: Hierarchy level plot for scattering off one oscillating square well. Each colored area represents the set of initial conditions that undergo a number  $N$  of collisions (transversals) within the well before exiting. Light blue corresponds to  $N$  greater or equal to 6. The white background is the set of initial conditions that transmit without any reflection. The parameters are:  $\eta_1 = 0.5$  and  $\eta_2 = 16.45$ .

With the help of hierarchy plots like Fig. 2 one can

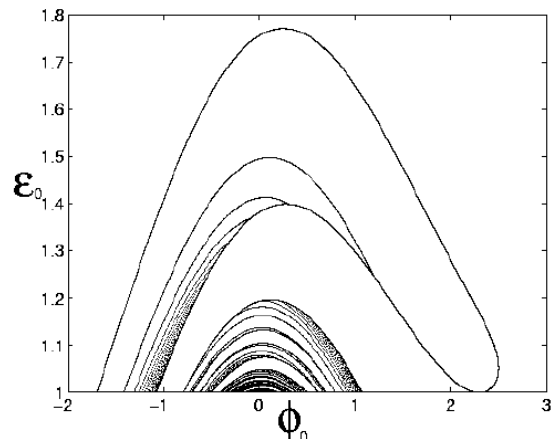


Figure 3: Boundaries between hierarchy levels for the single oscillating well. Same parameters as in Fig. 2. See text for an explanation on the construction of this plot.  $\eta_1 = 0.5$  and  $\eta_2 = 16.45$ .

easily determine for a given initial condition the outgoing energy and phase values, without having to iterate the map (11). One simply needs to locate the incoming asymptotes within its hierarchy level  $N$  and calculate Eq.(11) for the known value  $N$ . That is, knowledge of the initial conditions enables us not only to determine, but to *predict*, the scattering values for  $N$ ,  $\epsilon$  and  $\phi$ . However, for sufficiently low values of energy, the structure of the hierarchy levels in general becomes more intricate, requiring higher precision in the specification of the incoming asymptotes. Figs. 4a and 4b show, respectively, a plot of the number of collisions (transversals) and a plot of the final energy as a function of  $\phi_0$  for a fixed low incoming energy. The great sensitivity to initial conditions is further demonstrated by Figs. 5a-5d. Figure 5a is an example of how the number of collisions can gradually increase ( here in steps of 2) as  $\phi_0$  is varied over smaller and smaller intervals and then suddenly drops to  $N = 1$ , direct transmission. Fig. 5b shows the corresponding behavior of the final energy. Fig. 5c is an example of a typical situation where changes in the initial condition yield unpredictable, seemingly random, changes in the number of collisions and Fig. 5d is the corresponding behavior of the final energy.

The situation seems even more complex when the amplitude of oscillation is as large as the height of the static well, ( $\eta_1 = 1$ ). Figures 6 shows the rich structure of the response functions  $N(\phi_0)$  and the outgoing energy  $\epsilon(\phi_0)$ , due to the extreme sensitivity to initial conditions. Notice that this structure is nevertheless non-fractal. Numerically, the non-fractal structure is evident because of the absence of finer structures after increasing the resolution ( within numerical precision) enough times (see Fig. 7). Analytically, the fractal structure of the response ( or scattering) functions is ruled out by realizing that there are no hyperbolic

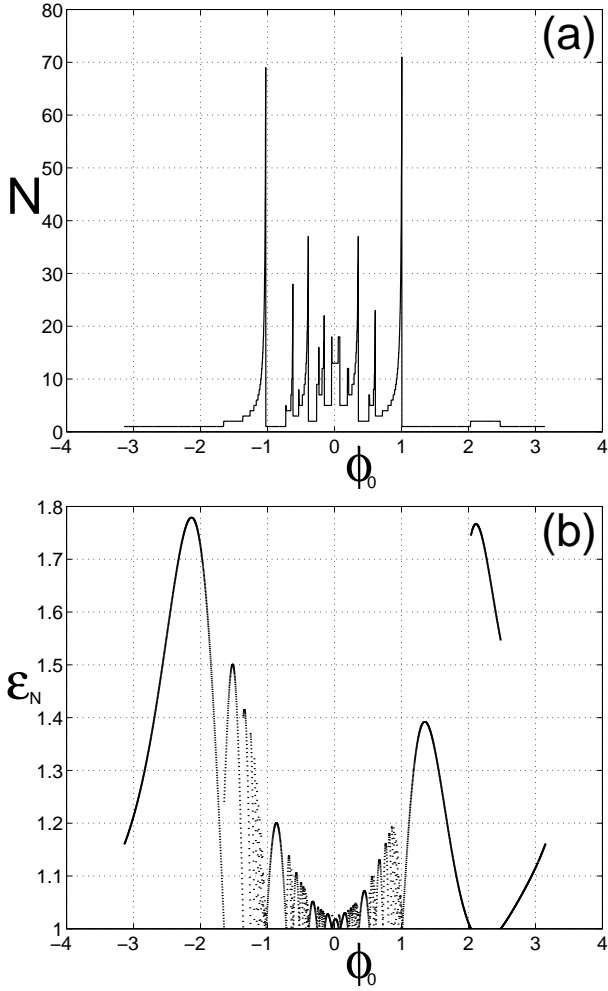


Figure 4: Scattering functions for the single oscillating well ( $\eta_1 = 0.5, \eta_2 = 16.45$ ). a) Number of collisions as a function of initial phase and b) final energy as a function of initial phase. The initial energy for all phases is  $\epsilon_0 = 1.025$ .

periodic points of the map. To see this consider the periodic orbits of period 1. The condition for period one orbits ( $\phi_1 = \phi_0, \epsilon_1 = \epsilon_0$ ) gives  $p^* = \frac{a\omega}{2\pi m}$ ,  $m \in \mathbb{Z}$ . Within the well,  $p^{*2}/2 + \eta_1 \cos(\phi) < 1$ , or,  $\cos(\phi) < \frac{1-p^{*2}/2}{\eta_1}$ . Hence, one can find an integer  $m$  for a given set of parameters ( $a, \omega$ , and  $\eta_1$ ) that satisfies the last inequality. This implies that there is a whole interval of the angle  $\phi$  that is periodic of period one. Furthermore, since the period one points come in one-parameter families, i.e., they are not isolated, these points cannot be hyperbolic nor elliptic. Therefore, they must be parabolic (see, e.g., [16]). A similar argument rules out the existence of higher periodic hyperbolic points. Topological chaos appears in systems having transverse homoclinic or heteroclinic connections (as this implies the existence of a Smale horseshoe) which in turn can exist if there are hyperbolic points [17]. Con-

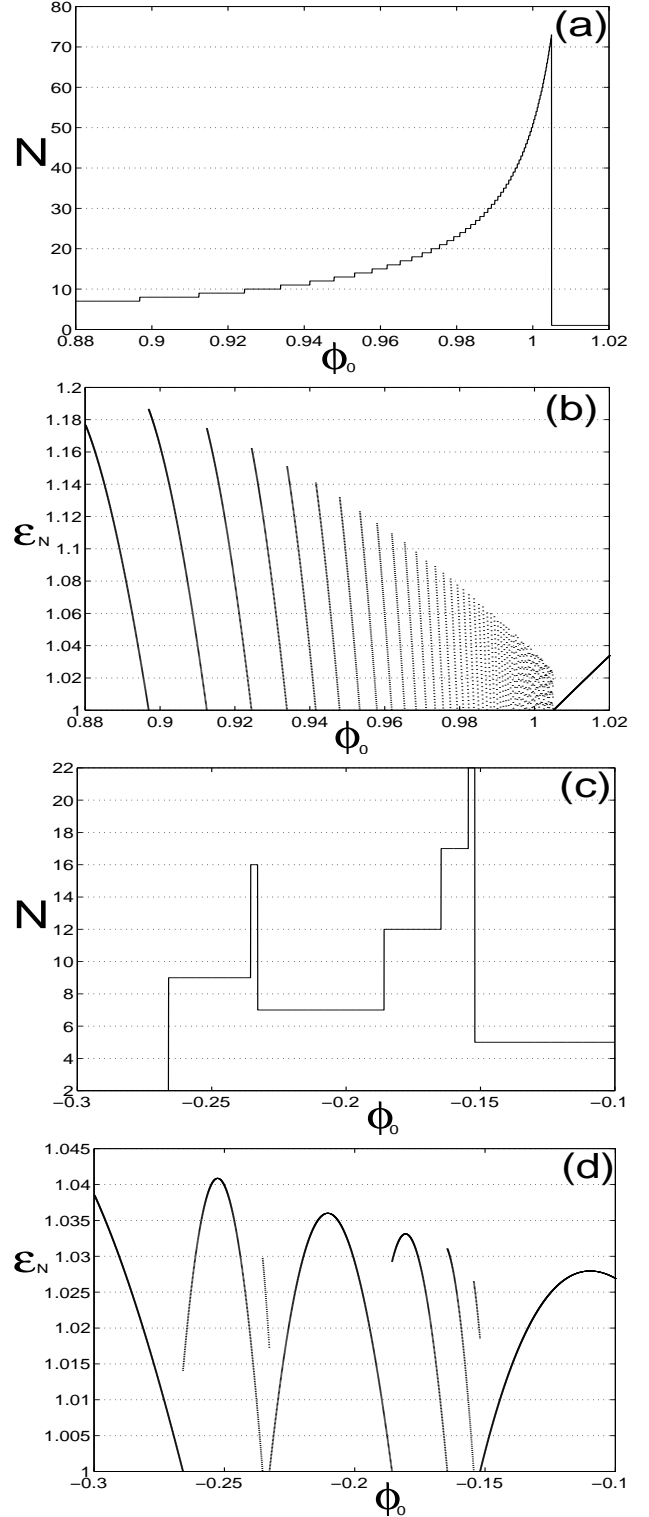


Figure 5: Scattering functions for the single oscillating well ( $\eta_1 = 0.5, \eta_2 = 16.45$ ) in two small ranges of initial phase. The ranges shown here correspond to magnifications of Figures 4a and 4b. Note the two different types of behavior, namely gradual change ((a) and (b)) and apparently random change ((c) and (d)) in the number of collisions as a function of initial phase.

sequently, there cannot be topological chaos in the case of a single well. Finally, if there is no topological chaos, there is no chaotic scattering.

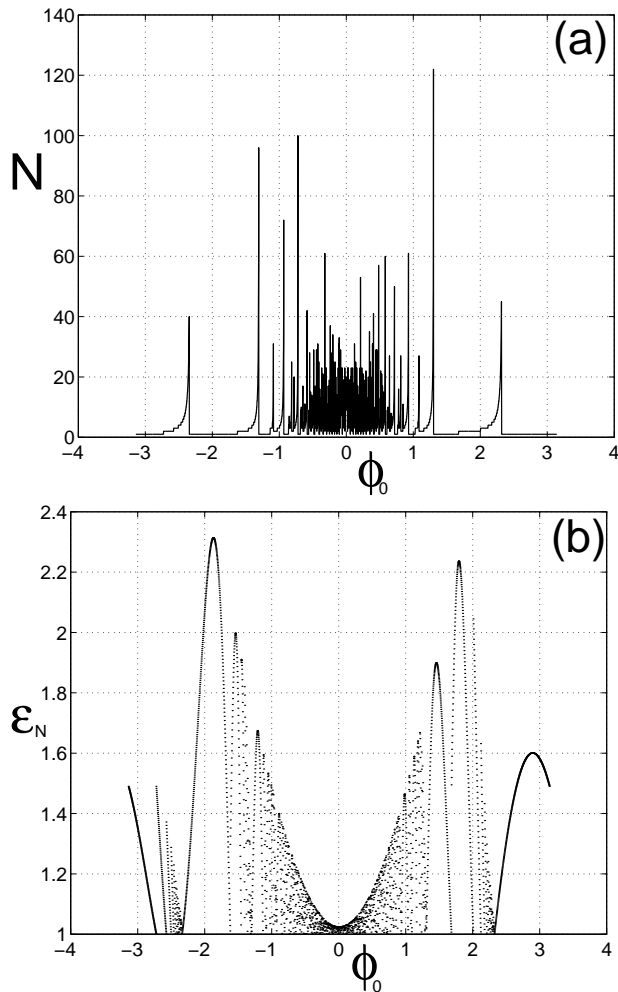


Figure 6: Scattering functions for the single well with  $\eta_1 = 1.0, \eta_2 = 16.45$ . a (b) is the number of collisions ( final energy) as a function of initial phase. The initial energy for all phases is  $\epsilon_0 = 1.025$ .

### 3 Two oscillating wells

Now we analyze the interaction of a particle with a potential formed by two neighboring wells, as shown in Fig. 8, oscillating in synchronization. The separation between the wells  $b$  is a new parameter that it is convenient to make dimensionless in the same way as was done for the well width  $a$ , namely,

$$\eta_3 \equiv \omega b / \sqrt{2V_0} \quad (12)$$

Assuming the particle approaches the two wells from the left and arrives at  $x = 0$  with energy  $\epsilon_0$  and phase  $\phi_0$ , it will exit the first well with energy and phase given by

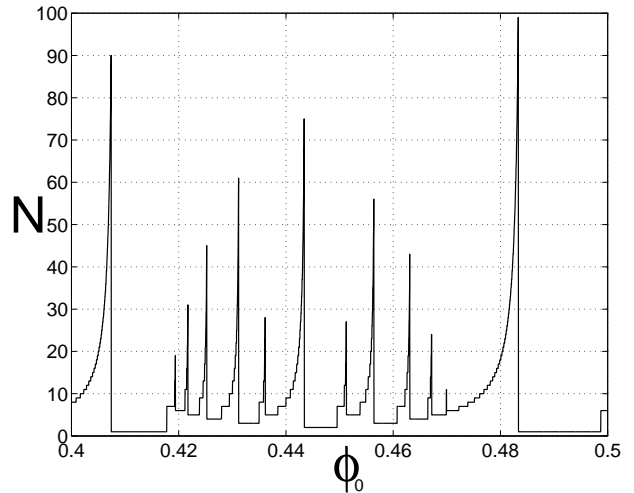


Figure 7: Magnification of the scattering function of Fig. 6.

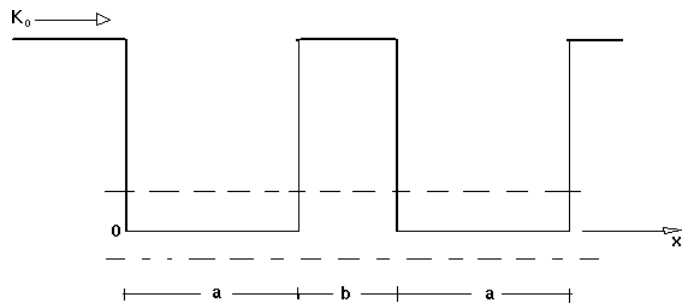


Figure 8: Schematic of the oscillating double well potential.

$$\begin{aligned} \epsilon_{m_1} &= \epsilon_0 + \eta_1 (\cos \phi'_{m_1} - \cos \Phi_0) \\ \phi'_{m_1} &= \Phi_0 + m_1 \Delta \Phi_0, \end{aligned} \quad (13)$$

where  $m_1$  stands for the number of transversals within well number one. The reason for using the new symbols, primed phase  $\phi'_{m_1}$  and capitalized phase  $\Phi_0$ , will become clear shortly. If  $m_1$  is even, the particle reflects from the first well and leaves the scattering region with energy  $\epsilon_{m_1}$  but if  $m_1$  is odd, the particle goes on to the second well. When it arrives at  $x = a + b$  the phase is

$$\Phi_{m_1} = \phi'_{m_1} + \delta \phi_{m_1}, \quad (14)$$

where

$$\delta \phi_{m_1} \equiv \eta_3 / \sqrt{\epsilon_{m_1} - 1}. \quad (15)$$

is the phase increase while the particle travels from  $x = a$  to  $x = a + b$ . Note that the primed phase labels the value of the phase right when the particle exits a well and the capitalized phase labels the phase as it enters the well. We shall use this convention throughout the rest of the paper.

After transversing the second well  $m_2$  times the particle exits with energy and phase given by

$$\begin{aligned}\epsilon_{m_2} &= \epsilon_{m_1} + \eta_1(\cos\phi'_{m_2} - \cos\Phi_{m_1}) \\ \phi'_{m_2} &= \Phi_{m_1} + m_2\Delta\Phi_{m_1}.\end{aligned}\quad (16)$$

If  $m_2$  is odd the particle exits the second well at  $x = a+b+a$ , leaving the interaction region, but if  $m_2$  is even the particle exits at  $x = a+b$ , returning toward the first well, and so on. Let  $m_i$  stand for the number of transversals within the well number  $i$ , where  $i$  odd (even) refers to well number one (two). We can then write

$$\begin{aligned}\epsilon_{m_n} &= \epsilon_{m_{n-1}} + \eta_1(\cos\phi'_{m_n} - \cos\Phi_{m_{n-1}}) \\ \phi'_{m_n} &= \Phi_{m_{n-1}} + m_n\Delta\Phi_{m_{n-1}},\end{aligned}\quad (17)$$

where

$$\Delta\Phi_{m_i} \equiv \eta_2/\sqrt{\epsilon_{m_i} - \eta_1\cos\Phi_{m_i}}\quad (18)$$

and  $m_i$  is even for all  $i$  except  $i = 1$  and  $i = n$  (The case  $m_1 = \text{even}$  is given by Eq. (13), where the particle did not interact with the second well).  $n$  labels the last well the particle crossed before leaving the interacting region and so is also the total number of interactions with the wells. On the other hand, the total number  $N$  of transversals is the sum of all  $m_i$  from  $i = 1$  to  $i = n$ . Figure 9 is the hierarchy plot computed for  $\eta_3 = 5$  and with  $\eta_1$  and  $\eta_2$  the same as for figure 2. Note that for two wells, a total number of  $N = 2$  transversals can be produced in two ways: either, two transversals in the first well with no interaction with the second well, or one transversal in the first well and one with the second well. Figure 9 associates the color blue to the latter possibility while the white area corresponds to the first possibility. Comparison with Fig. 2 shows that the smooth boundaries between various hierarchy levels now appear fragmented and the scattering functions are expected to show some evidence of this fragmentation. Figures 10a and 10b plot the energy and the number of collisions, respectively, as a function of the initial phase for the same parameters as those of Fig.9 and for an incoming energy  $\epsilon_0 = 1.025$ . At first sight the plots  $N(\phi_0)$  do not appear qualitatively different from those corresponding to a single well (Figs. 4 and 6) but a closer look reveals that as the resolution is increased there appears more and more structure, suggesting its fractality ( see Fig. 11). That such fractality exists can be demonstrated by considering the dynamics of particles initially placed between the wells. Let us first define the Poincare surface to be the midpoint between the two wells and positive momentum and choose the coordinates to be the energy and phase. The energy at the Poincare surface is given by the first of Eqs. (17) but the phase is shifted by half of  $\delta\phi_{m_n}$  to correspond to the midpoint between the wells. Thus, the Poincare map is

$$\epsilon_{m_n} = \epsilon_{m_{n-1}} + \eta_1(\cos\phi'_{m_n} - \cos\Phi_{m_{n-1}})$$

$$\phi_{m_n} = \phi'_{m_n} + \frac{1}{2}\delta\phi_{m_n}.\quad (19)$$

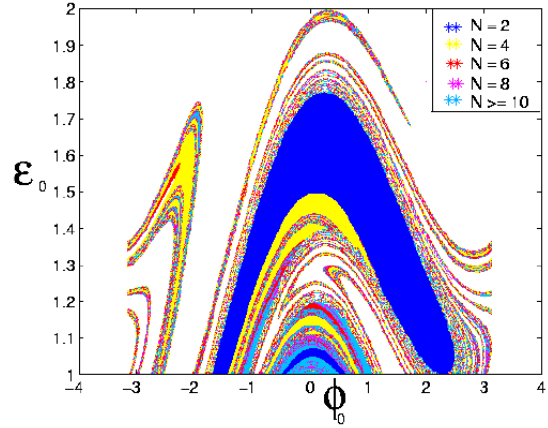


Figure 9: Hierarchy level plot for the oscillating double well. There are two ways of producing  $N = 2$  as mentioned in the text. The white area corresponds to direct transmission (one transversal in the first well and one in the second one). The blue area corresponds to two transversals in the first well and none in the second one. In general, there are  $2^{N/2}$  ways. Here all possibilities are plotted for  $N$  equal or greater than 4. The parameters are  $\eta_1 = 0.5$ ,  $\eta_2 = 16.45$ , and  $\eta_3 = 5$ .

We now place a set of initial conditions on a grid on this surface and let them evolve forward in time. Some initial conditions will leak after a finite number of interactions with one or both wells and some will remain trapped forever. Fig.12a is a plot for those orbits that return to the Poincare surface at least once and up to 1000 times. In Fig. 12b we plot only those orbits that returned to the surface at least 100 times and up to 1000 times. That is, transient orbits that crossed the Poincare surface less than 100 times were not plotted in Fig. 12b. Finally, in Fig. 13 we plot orbits that cross this Poincare section at least 4000 times and up to 5000 times. This Poincare plot now represents the dynamics of the particles that are trapped forever (bounded orbits) and shows the appearance of an island of stability associated with a fixed point of period one and the surrounding elliptic islands of higher period ( here period 8). This is just the common structure predicted by the Poincare-Birkhoff theorem [18] with alternating elliptic and hyperbolic fixed points. The hyperbolic points and their associated homoclinic/heteroclinic tangle are not shown in this figure. The outermost island chains are not screened behind a KAM curve, therefore the scattering flow can reach the homoclinic tangle. Correspondingly, the tendrils of the stable and unstable manifolds of this tangle reach out into the asymptotic region, thus producing the fractal structure of the scattering functions [19]. Hence, we have a numerically based proof that

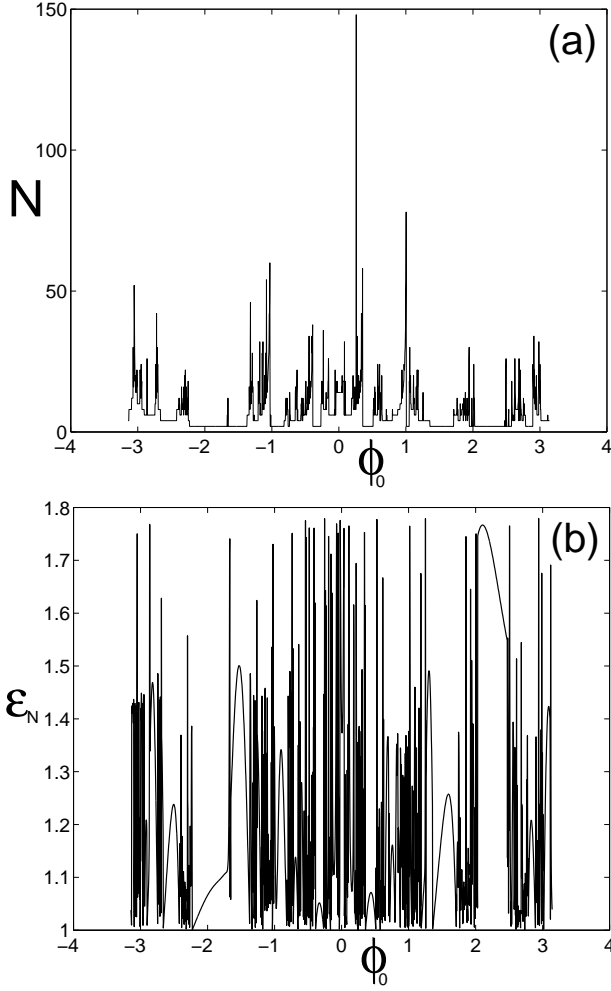


Figure 10: Scattering functions for the oscillating double well. a) Number of collisions as a function of initial phase and b) final energy as a function of initial phase. The initial energy for all phases is  $\epsilon_0 = 1.025$ .  $\eta_1 = 0.5$ ,  $\eta_2 = 16.45$ , and  $\eta_3 = 5.0$

a particle scattering off this double well oscillating potential gives rise to true chaotic scattering, unlike the case of a single well.

## 4 Oscillating chain

The infinite oscillating chain is formed by the infinite repetition of the double well arrangement and hence (19) is the Poincare map describing the motion of the particle, except that  $m_i$  has a different meaning now. Namely,  $m_i$  now stands for  $m_i$  transversals during the  $i$ th interaction of the particle with a well. Of course, here  $m_i$  can be odd or even for **any**  $i$ ,  $i = 1, 2, 3, \dots$ . Since the chain is periodic the Poincare plots are modulo  $a + b$ . Figures 14-17 show the Poincare plots for increasing values of  $\eta_3$  ( $\eta_1 = 0.5$ ;  $\eta_2 = 16.45$ ). In these figures the phase

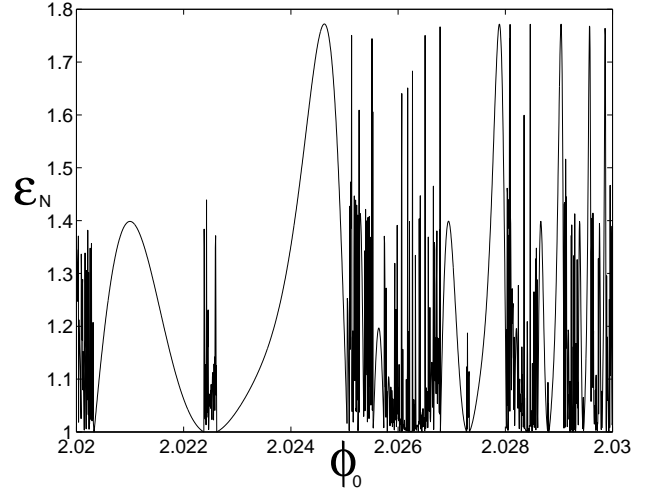


Figure 11: Magnification of Figure 10b.

points have been labeled  $(\epsilon_n, \phi_n)$ ,  $n = 1, 2, 3, \dots$  instead of  $(\epsilon_{m_n}, \phi_{m_n})$ ,  $n = 1, 2, 3, \dots$ , because these plots do not contain the information on how many transversals  $m_n$  occur for each interaction  $n$ .

For the analysis of these plots it is convenient to write the energy  $\epsilon_{m_n}$  of eq. (19) in terms of the initial conditions:

$$\begin{aligned} \epsilon_{m_n} &= \epsilon_0 + \eta_1(\cos\phi'_{m_n} - \cos\Phi_0) + \\ &\quad + \eta_1 \sum_{i=1}^{n-1} (\cos\phi'_{m_i} - \cos\Phi_{m_i}) \\ \phi_{m_n} &= \phi'_{m_n} + \frac{1}{2}\delta\phi_{m_n}. \end{aligned} \quad (20)$$

Another formula that will be useful below is obtained by substituting  $\phi'_{m_n} = \phi_{m_n} - \frac{1}{2}\delta\phi_{m_n}$  and  $\Phi_{m_n} = \phi_{m_n} + \frac{1}{2}\delta\phi_{m_n}$  in (20) and expanding the cosine terms:

$$\begin{aligned} \epsilon_{m_n} &= \epsilon_0 + \eta_1[\cos(\phi_{m_n} - \frac{1}{2}\delta\phi_{m_n}) - \cos\Phi_0] + \\ &\quad + 2\eta_1 \sum_{i=1}^{n-1} \sin\phi_{m_i} \sin\frac{1}{2}\delta\phi_{m_i} \end{aligned} \quad (21)$$

$$\begin{aligned} \phi_{m_n} - \frac{1}{2}\delta\phi_{m_n} &= \phi_{m_{n-1}} + m_n\Delta\Phi_{m_{n-1}} + \\ &\quad + \frac{1}{2}\delta\phi_{m_{n-1}} \end{aligned} \quad (22)$$

Some features of the Poincare plots for small  $\eta_3$  can be understood qualitatively by first analyzing the unperturbed case ( $\eta_3 = 0$ ). If  $\eta_3 = 0$  then  $\delta\phi_{m_i} = 0$ ,  $\Phi_{m_i} = \phi_{m_i} = \phi'_{m_i}$  for all  $i$ , and (21) and (22) reduce to

$$\epsilon_{m_n} = \epsilon_0 + \eta_1(\cos\phi_{m_n} - \cos\phi_0), \quad (23)$$

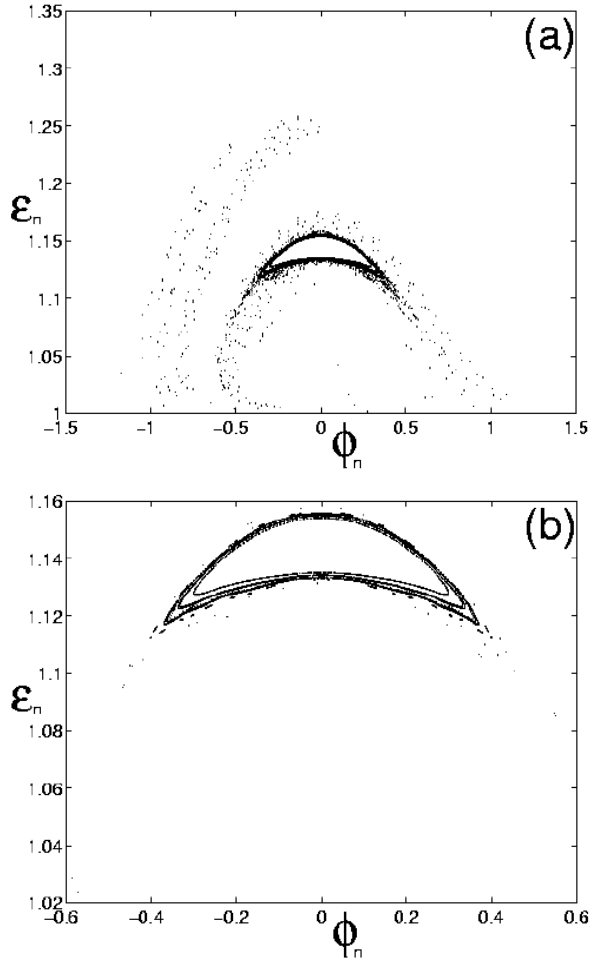


Figure 12: Transient and bound orbits for the oscillating double well. a) is the Poincaré plot for those orbits that return to the surface once and up to 1000 times; b) same as a) but plots only those that crossed the surface at least 100 times and up to 1000 times. Here  $\eta_2 = 6.28$ ,  $\eta_3 = 0.1$ , and  $\eta_1 = 0.5$

$$\begin{aligned}
 \phi_{m_n} &= \phi_{m_{n-1}} + m_n \Delta \phi_{m_{n-1}} \\
 &= \phi_0 + \Delta \phi_0 \sum_{i=1}^n m_i.
 \end{aligned}
 \tag{24}$$

To obtain the last equation we used the fact that  $\Delta \phi_{m_i} = \Delta \phi_0$  for all  $i$  since  $\epsilon_{m_i} - \eta_1 \cos \phi_{m_i}$  is the (adiimensional) internal kinetic energy, which is conserved for  $\eta_3 = 0$  ( see discussion below Eq. (1)). Eqs. (23) and (24) show that for  $\eta_3 = 0$  all orbits are described by invariant 1D curves, the cosine curves  $\epsilon_{m_n}(\epsilon_0, \phi_0)$ . Recall that for a given interaction  $n$  with a well  $\epsilon_{m_n} \geq 1$  but  $\epsilon_{m'_n} < 1$  for  $m'_n < m_n$ . It is clear from (23) that if  $\epsilon_0 > 1 + 2\eta_1$  then  $\epsilon_{m_n} > 1$  and  $m_n = 1$  for all  $n$  and hence the motion is of the *translational* type; the particle never changes direction. If  $\epsilon_0 = 1 + 2\eta_1$  then the right hand side of (23) can be as small as one for some  $n$ , provided  $\phi_0 = 0$  and

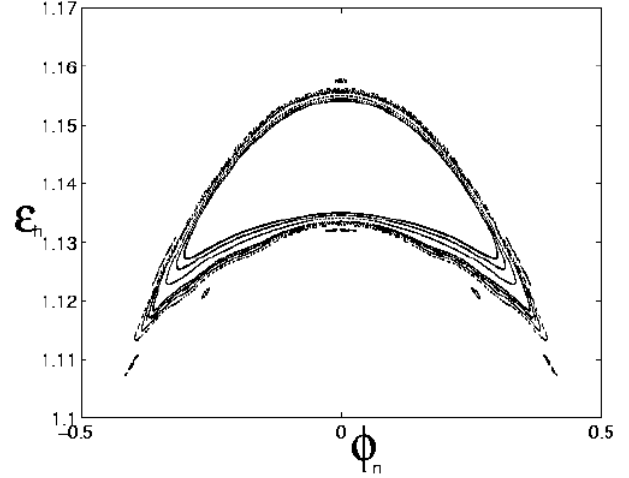


Figure 13: Poincaré plot for the oscillating double well. Here the minimum number of crossings can be as large as 5000 for some orbits. Orbits that left the interactions region before 4000 crossings are not plotted. Same parameters as Fig.12.

$\phi_{m_n} = k\pi$ ,  $k$ , odd. This implies that  $n\Delta\phi_0 = n\eta_2/\sqrt{1+\eta_1}$  must be exactly equal to  $k\pi$ , but for any  $\eta_1$  in the range  $(0, 1)$  and any  $\eta_2 \geq 0$ , there are some integers  $n$  and  $k$  that approximate arbitrarily close this equality. Since  $\epsilon = 1$  is the energy threshold, above which the particle does not reflect, then it follows that the curve  $\epsilon = 1 + \eta_1 + \eta_1 \cos \phi$  defines the *separatrix* curve, separating translational orbits from *librational* orbits ( curves below the separatrix). For initial conditions placed below the separatrix,  $m_n$  is in general larger than one. Since all curves, translational or librational, are invariant curves, there is no possibility for a translational orbit to become a librational one, and viceversa. The three top orbits of Fig. 14a are translational and the rest are librational.

Now consider the  $\eta_3 > 0$  case. Notice that the last term of (21) produces, as a function of  $\phi_{m_n} - \frac{1}{2}\delta\phi_{m_n}$ , fluctuations from the invariant cosine curve. These fluctuations can be small or large, depending on the value of  $\eta_3$  and whether the terms in the sum add constructively or destructively. Consider the case  $\eta_3 \ll 1$ . If in addition  $\delta\phi_{m_i} \ll 1$  for all  $i$  then the summation term can be approximated by  $\eta_1 \sum \sin \phi_{m_i} \delta\phi_{m_i}$ . The summed terms would yield an appreciable deviation from the cosine curve if  $\sin \phi_{m_i}$  were to oscillate slowly even if each term in the sum is small. This could happen for low energies ( c.f., (22) and (18)) and the orbit in the Poincaré surface will appear as scattered points in the neighborhood of the cosine curve. Similarly, if  $\epsilon_{m_i}$  is close to one, the last term of (19) may become the dominant term. Thus even for a small  $\eta_3$ , the perturbation can be strong for initial conditions in the neighborhood of the unperturbed separatrix or for initial conditions on low-lying unperturbed librational



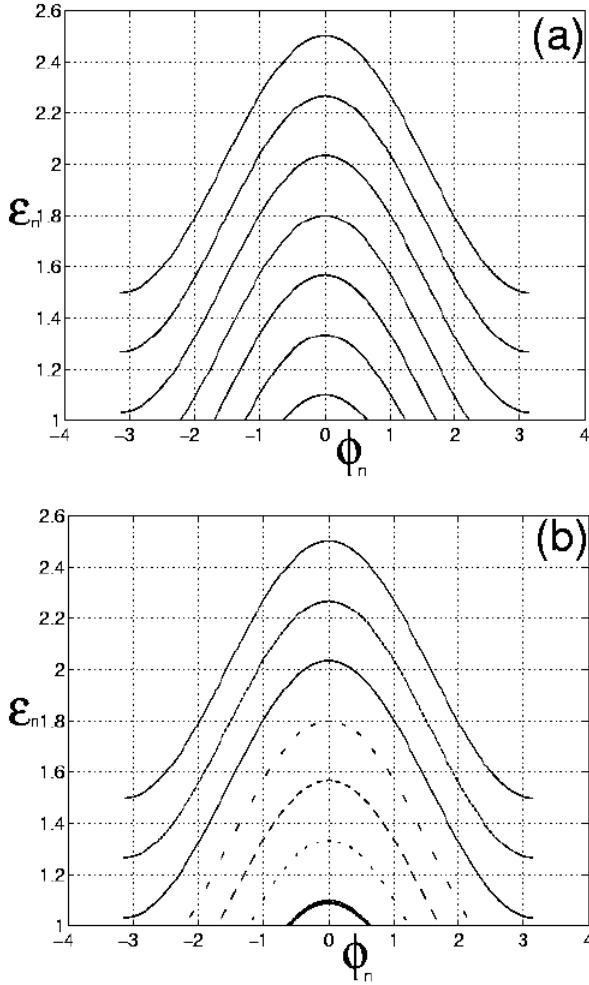


Figure 14: Poincaré plots for the oscillating chain of wells. a)  $\eta_3 = 0$  and b)  $\eta_3 = 0.0001$ .  $\eta_1 = 0.5$  and  $\eta_2 = 16.45$ .

orbits, see Fig. 14b. This is the concrete mechanism in this system for the appearance of chaotic orbits as  $\eta_3$  becomes slightly larger than zero ( Figs. 14b and 15).

Further analysis on the development of chaos as  $\eta_3$  is increased will be reported elsewhere. Here we shall only remark on some features observed in our numerical results ( Figs-15-17). It is interesting to note, for example, that the "boomerang" like stable island immersed in the chaotic sea of Fig. 15b ( at  $\epsilon_n \approx 1.2$ ) corresponds to the period one stable fixed point of the double well. In fact, the Poincaré plot for orbits trapped between two wells (see Fig.13) fits exactly within the abovementioned stable island of the chain, and the heteroclinic tangle of the double well lies on the chaotic sea of the chain. The elliptic islands above the lowest one most likely correspond to period one stable fixed points produced by trajectories trapped between three, four, and more wells.

Figures 15b to 17 show that as  $\eta_3$  continues to increase,

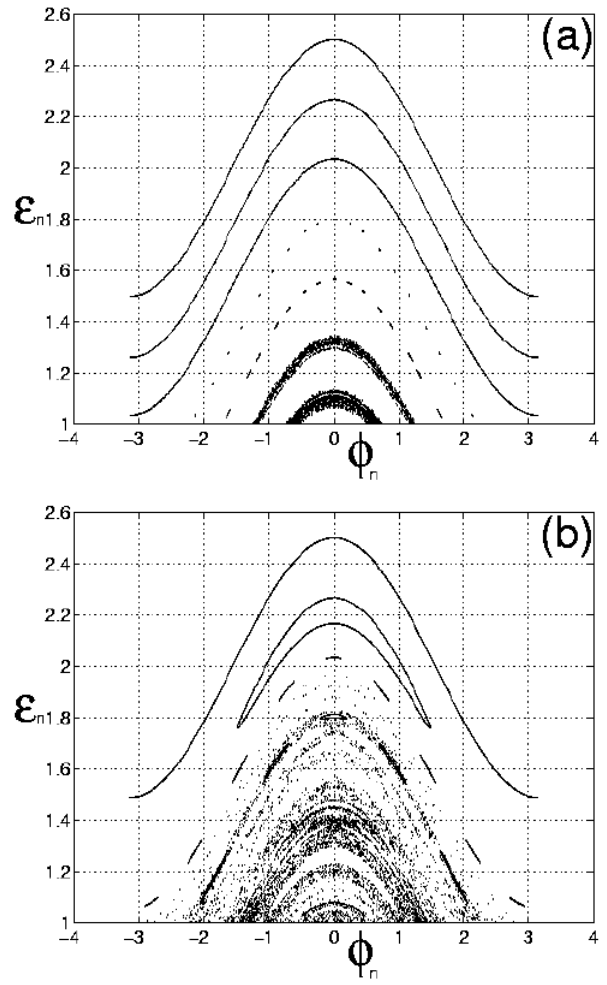


Figure 15: Poincaré plots for the oscillating chain of wells. a)  $\eta_3 = 0.001$  and b)  $\eta_3 = 0.01$ . Same  $\eta_1$  and  $\eta_2$  as in Fig. 14.

the chaotic area increases, allowing the energy to diffuse to higher and higher values. Thus if the energy is initially very small, after some time it may become very large as long as diffusion in energy is not limited by KAM curves.

In addition to energy diffusion, there is also diffusion in configuration space since the particle is interacting chaotically with the wells. Figure 18a plots the well number vs. number of interaction for the same parameters as in Fig. 17. Notice the random-walk-like behavior. That is, the particle, starting at well number one, seems to travel randomly forward and backward, returning repeatedly to the starting point. While this is happening, the energy of the particle oscillates wildly between one and approximately seven (see Fig. 18b). Then after approximately 55,000 interactions ( see Fig. 18b), the particle travels only in the negative direction during several interactions. This corresponds to a jump in its energy and the particle diffuses to higher energy values ( see Fig. 18b). This behavior

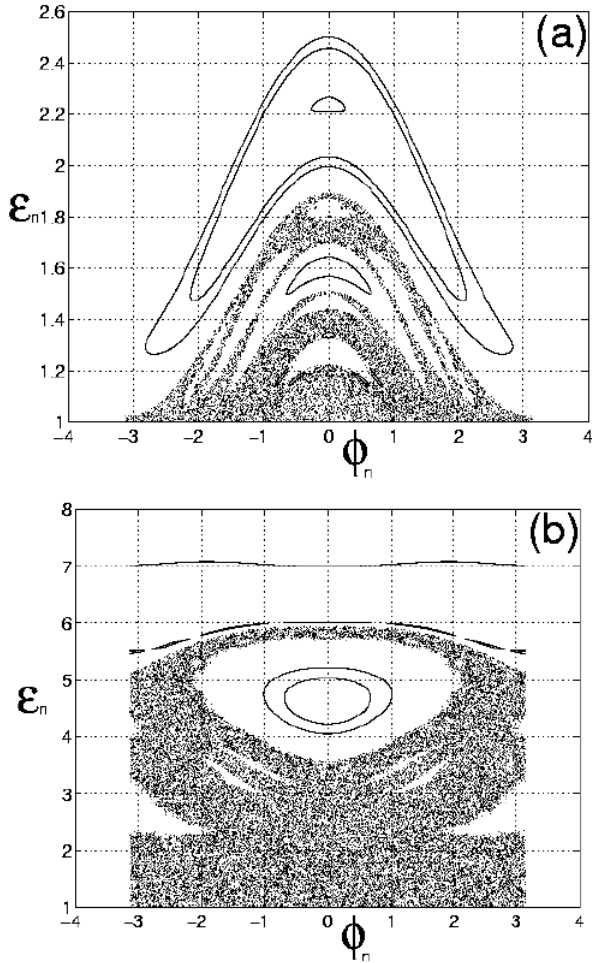


Figure 16: Poincaré plots for the oscillating chain of wells. a)  $\eta_3 = 0.1$  and b)  $\eta_3 = 10$ . Same  $\eta_1$  and  $\eta_2$  as in Fig. 15.

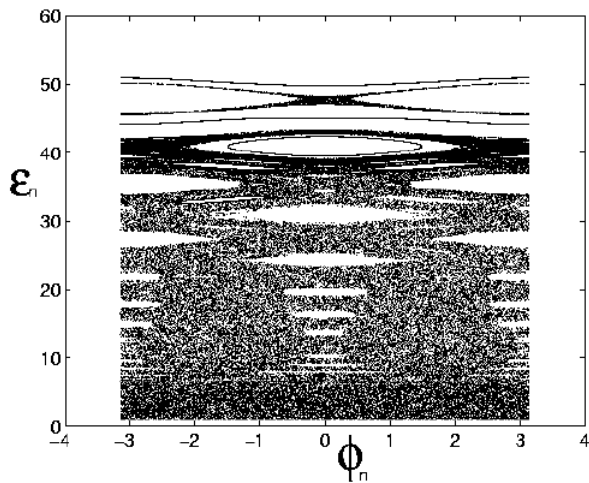


Figure 17: Poincaré plot for the oscillating well with  $\eta_3 = 500$ . Same  $\eta_1$  and  $\eta_2$  as in Fig. 16.

can be partially understood by examining the Poincaré plot of Fig.17. Notice that for energies around seven units, there are some visible white areas indicating the existence of some large, very thin, islands of stability, where the orbits get stuck temporarily. For larger number of interactions the particle eventually returns to the original well, performing a random-like-walk and the energy fluctuates over the whole range delimited by the KAM curve found around  $\epsilon = 42$ .

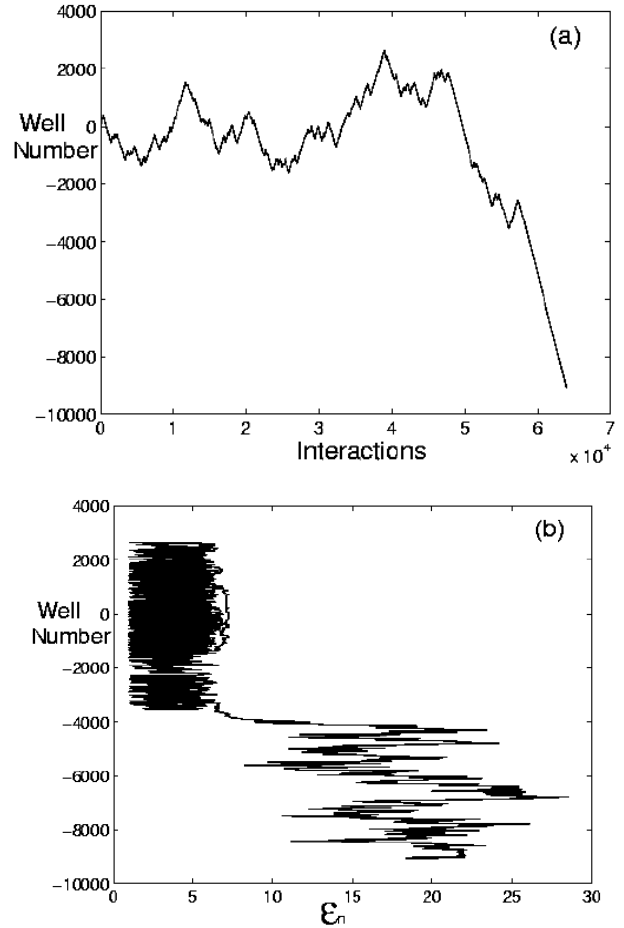


Figure 18: Space and energy diffusion in the oscillating chain. a) is diffusion in space, represented by the well number and b) is diffusion in energy of the particle as it interacts with the various wells. The parameters are  $\eta_1 = 0.5$ ,  $\eta_3 = 16.45$ , and  $\eta_3 = 500$ .

## 5 Conclusions

In this paper we have described the motion of a classical particle interacting with one, two, and finally an infinite chain of oscillating square wells. For the single well we found that although the scattering functions, such as final energy and number of collisions as a function of initial conditions, may yield complex behavior, extremely sensitive

to initial conditions ( hence unpredictable), the nonexistence of hyperbolic fixed points renders the scattering non-chaotic. On the other hand, when the potential region is formed by two oscillating wells, the scattering functions are truly fractal as expected since it was shown that there exists topological chaos. The dynamics of a particle interacting with a chain of oscillating wells was shown to yield the transition to chaos as the separation between the wells increases. Although there is chaotic diffusion in energy this is limited by KAM curves and the diffusion in configuration space is random-like but with some peculiarities. The scattering off one and two oscillating square wells has been considered previously by some authors to model some microscopic and mesoscopic systems but their treatments have been completely quantum mechanical. Here we treat the purely classical description as a starting point to understand their classical-quantum correspondence. The oscillating chain represents a classical oscillating Kronig-Penney model, particularly relevant to solid state systems, and it may help in the understanding of some quantum properties. For example, some localization of the wave function of an electron in a one-dimensional crystal or in a superlattice in the presence of some monochromatic field [20] is expected to occur since we have shown that the motion can be chaotic. This should manifest itself in the reduction of conductivity. Thus, there is some similarity with the Anderson Model [21]. The dynamics of a particle in the oscillating chain is also similar to the Fermi accelerator model, with the additional nice feature that in the chain there is diffusion in space as well as in energy. Finally, as far as the energy is concerned the oscillating chain is equivalent to a single oscillating well inside a larger static infinite square well. An oscillating square barrier inside a larger static infinite square well has been recently considered in [22].

**Acknowledgments:** We thank Luis Benet for illuminating discussions. This work was partially supported by CONACYT (Mexico) grant, No. 26163-E and NSF-CONACYT, grant No. E120.3341

## References

- [1] W. Cai, P. Hu, T.F. Zheng, B. Yudanin, and M. Lax, *Phys. Rev. B* **41**, 3513 (1990).
- [2] G. Burmeister and K. Maschke, *Phys. Rev. B* **59**, 4612 (1999).
- [3] M. Wagner, *Phys. Rev. B* **57**, 11899 (1998).
- [4] G. P. Berman, E. N. Bulgakov, D. K. Campbell, and A. F. Sadreev, *Physica B* **225**, 1 (1996).
- [5] W. Li and L.E. Reichl, *Phys. Rev. B*, to appear (1999)
- [6] F.Haake, *Quantum signatures of Chaos* (Springer-Verla, Berlin, 1991); L.E. Reichl, *The Transition to Chaos in Conservative Classical Systems; Quantum Manifestations* (Springer-Verlag, New York,1992); M.C. Gutzwiller, *Chaos in Classical and Quantum Mechanics* (Springer-Verlag, New York, 1990); and K. Nakamura, *Quantum Chaos: a New Paradigm on Nonlinear Dynamics* (Cambridge University Press, New York, 1993).
- [7] A.M.Chang, H.U. Baranger, L.N. Pfeiffer, and K.W. West, *Phys. Rev. Lett.* **73**, 2111 (1994); H.U. Baranger, *Physica D* **83**, 30 (1995), and references therein.
- [8] C.M. Marcus, A.J. Rimberg, R.M. Westervelt, P.F. Hopkins, and A.C. Gossard, *Phys. Rev. Lett.* **69**, 506 (1992)
- [9] G.A. Luna-Acosta, A.A. Krokhin, M.A. Rodriguez, and P.H.. Hernandez-Tejeda, *Phys. Rev.B* **54**,11410 (1996).
- [10] See, e.g., L.P. Kouwenhoven, S. Jauhar, J. Orenstein, P.L. McEuen, Y. Magamune, J. Motohisa, and H. Sasaki, *Phys. Rev. Lett.***73**, 3443 (1994).
- [11] R.H. Blick, R.J. Haug, D. W, van der Weide, K. von Klitzing, and K. Eberl, *Appl. Phys. Lett.* **67**, 3924 (1995); and H. Drexler, J.S. Scott, S.J. Allen, K.L. Campman, and A.C. Gossard, *Appl. Phys. Lett.* **67**, 2816 (1995).
- [12] W. Cai, T.F. Zheng, P. Hu, B. Yudanin, and M. Lax, *Phys. Rev. Lett.* **63**, 418 (1989); Y. Fu and M. Willander, *J. Appl. Phys.* **74**, 3264 (1993); F. Rojas and E. Cota, *J. Phys.: Condens. Matter* **5**, 5159 (1993); and B. Y. Gelfand, S. Schmitt-Rink, and A. F. J. Levi, *Phys. Rev. Lett.* **62**, 1683 (1989).
- [13] See, e.g., Q-f. Sun, J. Wang, and T-h. Lin, *Phys. Rev. B* **58**, 13007 (1998); M. Wagner, *Phys. Rev. Lett.* **76**, 4010 (1996); and B. J. Keay, S. J. Allen, J. Galán, J. P. Kaminski, K. L. Campman, A.C. Gossard, U. Bhattacharya, and M. J. W. Rodwell, *Phys. Rev. Lett.* **75**, 4098 (1995).
- [14] See for example, page 474 in P.Y. Yu and M. Cardona, *Fundamentals of Semiconductors*, 2nd edition (Springer-Verlag, Berlin, 1999).
- [15] C. Jung and H-Jcholz, *J.Phys. A: Math. Gen.***21**, 2301 (1988).
- [16] M. Tabor, *Chaos and integrability in Nonlinear Dynamics. An Introduction*, (John Wiley and Sons, Inc., 1989).
- [17] S. Wiggins, *Introductions to Applied Nonlinear Dynamical Systems and Chaos*, (Springer-Verlag, New York, 1990).

- [18] A.J. Lichtenberg and M.A. Lieberman, *Regular and Stochastic Motion* (Springer, New York, 1983).
- [19] For a recent review of chaotic scattering see the Special issue on Chaos, Vol. 3, No. 4, see also C. Jung and P.-H. Richter, *J. Phys A: Math. Gen.* **23**, 2847 (1990).
- [20] F.G. Bass and A.P. Tetervov, *Phys. Rep.* **140**, 237 (1986); V.V. Pavlovich and E.M. Epshtein, *Sov. Phys. Semicond.*, **10**, 1196 (1976); M. Holthaus and D. Hone, *Phys. Rev.* **B 47**, 6499 (1993); and K. N. Alekseev, G. P. Berman, D.K. Campbell, E. H. Cannon, and M.C. Cargo, *Phys. Rev.* **B 54**, 10625 (1996).
- [21] P. W. Anderson, *Phys. Rev.* **109**, 1492 (1958) and P.A. Lee and T.V. Ramakrishnan, *Rev. Mod. Phys.* **57**, 287 (1985); and for dynamical localization, see F.M. Izrailev, *Phys. Rep.* **196**, 299 (1990) and references therein.
- [22] J. L. Mateos and J.V. Jos, *Physica A* **257**, 434 (1998).